Bioelectrochemistry 100 (2014) 105–111

Contents lists available at ScienceDirect

Bioelectrochemistry

journal homepage: www.elsevier.com/locate/bioelechem

Tissue damage modeling in gene electrotransfer: The role of pH

N. Olaiz [a,1], E. Signori [b,1], F. Maglietti [a], A. Soba [a], C. Suárez [a], P. Turjanski [a], S. Michinski [c], G. Marshall [a,*]

[a] Laboratorio de Sistemas Complejos, Departamento de Computación, FCEyN, Universidad de Buenos Aires, C1428EGA Buenos Aires, Argentina
[b] Laboratory of Molecular Pathology and Experimental Oncology, CNR-IFT, Rome, Italy
[c] Instituto Tecnológico de Buenos Aires, Argentina

ARTICLE INFO

Article history:
Received 28 June 2013
Received in revised form 22 April 2014
Accepted 2 May 2014
Available online 14 May 2014

Keywords:
Gene electrotransfer
pH
Hyaluronidase
Computational modeling

ABSTRACT

Optimal gene electrotransfer (GET) requires a compromise between maximum transgene expression and minimal tissue damage. GET in skeletal muscle can be improved by pretreatment with hyaluronidase which contributes to maximize transgene uptake and expression. Nevertheless, tissue damage remains severe close to the electrodes, with a concomitant loss of GET efficiency. Here we analyze the role of pH in tissue damage in GET protocols through in vivo modeling using a transparent chamber implanted into the dorsal skinfold of a mouse (DSC) and intravital microscopy, and in silico modeling using the Poisson–Nernst–Planck equations for ion transport. DSC intravital microscopy reveals the existence of pH fronts emerging from both electrodes and that these fronts are immediate and substantial thus giving rise to tissue necrosis. Theoretical modeling confirms experimental measurements and shows that in GET protocols whether with or without hyaluronidase pretreatment, pH fronts are the principal cause of muscle damage near the electrodes. It also predicts that an optimal efficiency in GET protocols, that is a compromise between obtaining maximum electroporated area and minimal tissue damage, is achieved when the electric field applied is near 183 V/cm in a GET protocol and 158 V/cm in a hyaluronidase + GET protocol.

1. Introduction

During the last decade, pulsed electric fields were explored in different scientific domains such as medicine, biotechnology and environmental preservation [1]. In the medical field, treatments of tumors based on electroporation or electropermeabilization (EP), a technology in which cell membrane integrity is disturbed with an electric field, are emerging. Different approaches are electrochemotherapy (ECT), irreversible electroporation (IRE) and gene electrotransfer (GET). ECT, [2–4], combines reversible electroporation with non-permeant anticancer drugs to potentiate their entry into the cell. IRE, [5], is a technique that kills cells leaving intact extracellular matrix, vessels and nerves. GET, [6,7], has great potential as a non-viral gene-delivery system as it achieves the introduction of plasmids or oligonucleotides into the cells. After the development of EP devices this technique became widespread for delivering molecules inside the cell. Although the mechanisms of GET have not been completely clarified [8], it is supposed that a higher DNA uptake in vivo is possible thanks to the enhancement of cell membrane permeabilization and electrophoretic movement of DNA molecules into the target cells. The effect of electrophoresis on GET efficiency was presented in [9] using different combinations of high and low voltage pulses.

Moreover, if GET is applied to muscle cells, it works in favoring the antigen production within the skeletal muscle [10], and in the activation of pro-inflammatory pathways and in the recruitment of cells involved in antigen presentation [11]. This mechanism turns GET into a useful strategy in DNA vaccination protocols, and a promising approach for the introduction of foreign antigens into the host for inducing an immune response not only against infectious diseases but also against malignant tumors [12].

Since GET is also associated with some tissue damage that must be minimized, optimal GET requires a compromise between maximum transgene expression and minimal tissue damage. In [13,14] it was shown that GET in skeletal muscle can be improved by pretreatment with hyaluronidase, an enzyme able to degrade hyaluronan, an ubiquitous glycosaminoglycan molecule of the extracellular matrix surrounding muscular fibers and skin [15]. This treatment leads to a better penetration and spread of DNA into the muscle tissue coupled with a reduction of muscle damage.

Even if the use of pre-treatment by hyaluronidase reduces muscle fiber damage, traces of necrosis still remain visible in the tissue with a concomitant loss of muscle fibers and a reduction in transgenic gene expression. It has been suggested that both effects (uncontrolled necrosis and loss of efficiency) may be strongly dependent on pH alterations induced by electrolysis [16–19]. Significant pH changes of the medium may induce deleterious effects on the plasmids used in GET, as DNA denaturation is prominently affected by pH. Plasmids are usually denatured when exposed to an alkaline medium above 8.4, and it takes less

* Corresponding author. Tel.: +54 11 4576 3390x709; fax: +54 11 4576 3359.
E-mail address: marshallg@arnet.com.ar (G. Marshall).
[1] These two authors contributed equally to this work.

http://dx.doi.org/10.1016/j.bioelechem.2014.05.001
1567-5394/

than 1 s to permanently denature them at pH = 12.5. In fact, results presented in [20] show that extreme pH changes occur in tissues when GET pulses are applied, in spite of the presence of natural buffers. Thus, it seems relevant to quantify the extent and evolution of these pH changes during GET. A way to reduce their effects could be the minimization of voltages and pulse number and the maximization of pulse length as far as possible. Actually, this new low-current, low-voltage and long-duration pulse procedure, was recently proved to be safer and more efficient in GET [21].

The aim of this work was to study through in vivo and in silico modeling the role of pH in tissue damage in hyaluronidase + GET protocol applications, we will show that it is mainly due to the presence of strong pH effects. The final goal is to improve gene delivery protocols by maximizing electroporated area and minimizing pH effects through pulse parameters selection.

2. Materials and methods

2.1. In vivo modeling

2.1.1. Measurements in tibialis anterior muscle (TAM)

Part of the experimental work presented here for assessing the effect of field strength on damage and expression, corresponds to data extracted from [13]. In those experiments, groups of four male F1 mice were injected in TAM with bovine hyaluronidase and plasmid followed by a GET protocol (200, 175, 150, 125, 100 and 0 V/cm with 8 pulses of duration 20 ms, with a distance between electrodes of 0.003 m). Pulses were applied with a BTX ECM 830 Harvard Apparatus, USA. More details can be found in the paper mentioned above.

With the purpose of extending data from [13], a new set of experiments was carried out in which a group of 10 female mice (6- to 8-weeks-old BALB-c/J) was injected in the TAM with bovine hyaluronidase (SIGMA, Catalog Number H4272) and plasmid DNA followed by a GET protocol identical to that used in [13]. In this experiment, we were not focused in the transfection efficiency (already evaluated and reported in [13]). The aim of this experiment was to reproduce the experiment reported in [13] for evaluating the electrical parameters which were necessary for the calibration of the mathematical models presented in this work. These parameters had not been measured in [13]. During our GET-type protocol experiments, electric current and voltage were measured with a digital oscilloscope (InfiniiVision DSO-X 2012A-SGM, Agilent Technologies, USA).

2.1.2. Measurements in dorsal skinfold chambers (DSC)

Due to the impossibility of observing and quantifying the extension of pH fronts in TAM, a substitute in vivo model was introduced. This consists in a transparent thin plastic chamber implanted into the dorsal skinfold of the mouse in which pH fronts are visualized with intravital microscopy. DSC is used in vivo studies and recent papers report this methodology. Intravital microscopy at the single vessel level brings new insights of vascular modification mechanisms induced by electropermeabilization [22,23].

In this context, a new set of measurements with intravital microscopy was carried out in DSC implanted in 10 female mice (6- to 8-weeks-old BALB-c/J) under general anesthesia, Ketamin/Xilacin (RICHMOND Argentina), Flumixin meglumine (analgesic, RICHMOND Argentina) and Enrofloxacin (antibiotic, RICHMOND Argentina). Then, 25 μl fluorescein isothiocyanate-dextran (FITC-Dextran (250 mg/kg), mass weight 70,000 Da SIGMA, Catalog Number 46945) in normal saline, used as tissue pH indicator, was injected intravenously through the tail. GET pulses (voltages of 100 and 300 V/cm and pulses with a duration of 20 ms at 1 Hz) were applied using electrodes inserted through the skin (thickness 0.6 mm). These electrodes consisted in two 27-gauge needles (separated a distance of 2 mm). A video camera was used to record pH front evolution in space and time during pulse application.

For a better visualization of pH fronts in the image presented in Fig. 3(a), Phenolphthalein ($C_{20}H_{14}O_4$) as acid base indicator (point transition at pH 8.3 approximately, SIGMA) and phenol red ($C_{19}H_{14}O_5S$) as acid base indicator (6.8–8.2, yellow to red, SIGMA), were applied topically, prior to the application of the GET protocol. Conductive gel was used on the electrode to ensure good electrical contact as commonly performed in GET protocols to allow the electric conductance. No plasmid vector neither hyaluronidase were injected into the DSC, we only applied the same electrotransfer conditions used in the in vivo pre clinical protocols carried out in the lab of one of the authors.

Animals were maintained in accordance with current regulations and standards of the NIH. Experimental protocols were designed according to the regulations of the committee for the care and use of laboratory animals of our institution (CICUAL).

2.2. In silico modeling

In silico modeling aimed at predicting the effect of the electric field on electroporated and damaged areas, in particular, the role of pH, in the application of a hyaluronidase + GET protocol to TAM and DSC. It is based on a macroscopic description of TAM and DSC experimental results. The damaged area is computed via the Poisson and Nernst–Planck (PNP) equations governing the electric field and the ion transport, respectively, in a four-component electrolyte (proton, hydroxide, chloride and sodium) and its numerical solution by deterministic finite differences. A change in the medium describes the presence or absence of hyaluronidase. Ion diffusion coefficients were adequately reduced following experimental data. The electroporated area is computed neglecting ion transport, assuming ohmic behavior and using the nonlinear Laplace equation governing the electric field, and its numerical solution by finite elements.

2.2.1. Governing equations

In the following we address the computation of the damaged area. A geometric definition of the problem is presented in Fig. 1. The x-axis aligns with the direction of the applied electric field. Assuming the validity of ion transport equations in an electrolyte, the flow density vector is defined as:

$$|j_i(x,t)| = \frac{1}{A}\frac{\partial n_i}{\partial t} \tag{1}$$

where j [mol/(cm^2 · s)] is the total ionic flux density through the area A [cm] normal to the direction of the electric field, n_i [mol] is the mole flux of the ionic species i (H^+, OH^-, Cl^- and Na^+), x [mm] and t [s] are the space and time coordinates, respectively. Assuming that ion transport is solely governed by diffusion and migration, the molar concentration

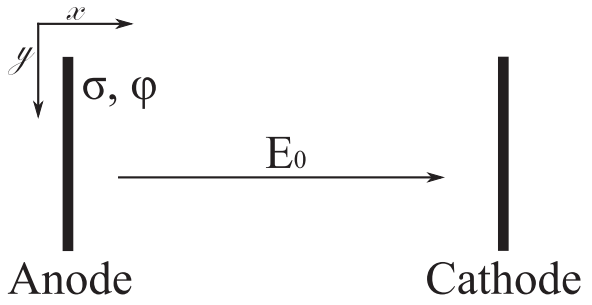

Fig. 1. A cross section in the x–y plane of the model geometry for TAM (parallel-plate electrodes) and DSC (parallel-needle electrodes). The x-axis is aligned with the direction of the electric field.

$C_i = n_i/V$ [mol/dm^3] where V is the volume, can be expressed via the Nernst–Planck (NP) equation as:

$$J_{i_{NP}}(x,t) = -D_{i_{NP}}\nabla C_{i_{NP}} - \frac{z_{i_{NP}}}{|z_{i_{NP}}|}u_{i_{NP}}C_{i_{NP}}\nabla\phi \tag{2}$$

where $C_{i_{NP}}$ [mol/dm^3], $D_{i_{NP}}$ [cm^2/s], $z_{i_{NP}}$ and $u_{i_{NP}}$ [cm^2/(V · s)] are the concentration, diffusion coefficient, charge number (with sign) and mobility of the species i_{NP}, respectively ($i_{NP} = H^+, OH^-$ and Cl^-).

The concentration of the fourth specie, (Na^+) is obtained via the electroneutrality condition:

$$\sum_{\substack{i = H^+, OH^-,\\ Cl^-, Na^+}}^{4} z_i C_i = 0. \tag{3}$$

The material balance for species i is given by

$$\frac{\partial C_i}{\partial t} + \nabla \cdot J_{i_{NP}}(x,t) = R_{i_r} \tag{4}$$

where R_{i_r} represents the production of species i_r through chemical reactions in the electrolyte.

2.2.2. Electrochemical reactions

Water proteolysis reaction is the only homogeneous chemical reaction considered:

$$H^+ + OH^- \underset{k_{w,f}}{\overset{k_{w,b}}{\rightleftharpoons}} H_2O$$

where $k_{w,b}$ and $k_{w,f}$ are the backward and forward dissociation constants of water, respectively. Input data and constants used in the numerical model can be found in [19].

This reaction is described by

$$\frac{\partial[H^+]}{\partial t} = \nabla\cdot\left(-D_{H^+}\nabla[H^+] - \frac{z_{H^+}}{|z_{H^+}|}u_{H^+}[H^+]\nabla\phi\right) - k_{w,b}[H^+][OH^-] + k_{w,f}[H_2O], \tag{5}$$

$$\frac{\partial[OH^-]}{\partial t} = \nabla\cdot\left(-D_{OH^-}\nabla[OH^-] - \frac{z_{OH^-}}{|z_{OH^-}|}u_{OH^-}[OH^-]\nabla\phi\right) - k_{w,b}[H^+][OH^-] + k_{w,f}[H_2O] \tag{6}$$

$$\frac{\partial[Cl^-]}{\partial t} = \nabla\cdot\left(-D_{Cl^-}\nabla[Cl^-] + \frac{z_{Cl^-}}{|z_{Cl^-}|}Fu_{Cl^-}[Cl^-]\nabla\phi\right). \tag{7}$$

In addition, the current density, J, is calculated from the flux of the sum of charged species (Faradays Law). The electrostatic potential is computed via the equation of charge conservation $\nabla \cdot J = 0$. Further details can be found in [19].

The computation of the electroporated area is treated via the solution of the nonlinear Laplace equation governing the electrostatic potential

$$\nabla \cdot J = \nabla \cdot (\sigma(|\nabla\phi|, Hyalu), \phi) = 0 \tag{8}$$

where J is the Ohmic current density, σ is the electric conductivity, ϕ is the electrostatic potential. σ is a function of the electric field and the presence or absence of hyaluronidase in the medium.

2.2.3. Numerical implementation

The damaged zone is determined by the pH variation which in turn is obtained by solving the PNP equations with the assumption of electroneutrality, following [18]. In this case, the PNP system of partial differential equations can be approximated by a split model describing ion transport in a two-step procedure. During the ON-time step, electric current is present and transport is governed by migration and diffusion; during the OFF-time step electric current is absent and transport is governed solely by diffusion. This splitting mechanism results in a multi-time step model in which the ON-time steps are several orders of magnitude smaller than the OFF-time step.

The split system of partial differential equations is solved, successively in time, in a two-step procedure (ON-time and OFF-time steps), in a fixed domain on a two-dimensional space-time uniform grid

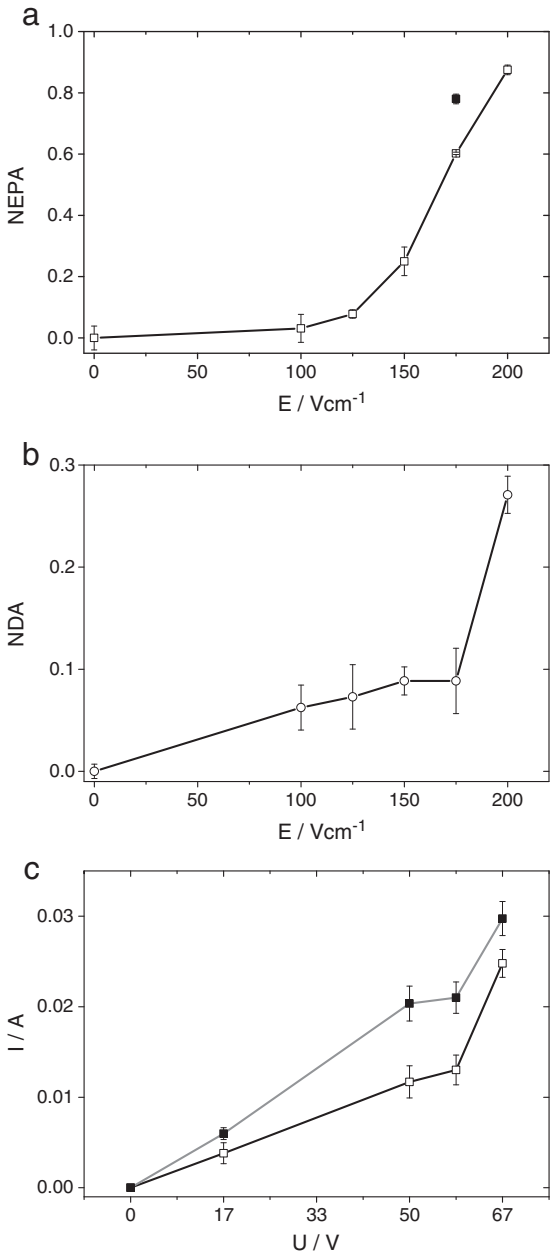

Fig. 2. (a) Normalized electroporated area (NEPA) in TAM (without hyaluronidase: hollow squares, with hyaluronidase: solid squares) vs. electric field E (V/cm). (b) Normalized damaged area (NDA) in TAM (without hyaluronidase) vs. electric field E (V/cm). (c) Electric current I(A) in TAM (without hyaluronidase: hollow squares, with hyaluronidase: solid squares) vs. voltage U (V).

using strongly implicit finite differences (details can be found in [24]). During the ON-time step, the time step is diminished several orders of magnitude to account for the migration in the microsecond scale, yielding a remarkable robust numerical algorithm. The computational model was written in the C++ language and implemented on an Intel(R) Core(TM) i5 class computer under Ubuntu Linux OS. The nonlinear equation resulting from the approximation of the boundary conditions is solved by the Newton's method, using Multidimensional Root-Finding routines from the GNU Scientific Library (GSL). Details of the whole procedure can be found in [18].

Simulation starts with the ON-time step system. At $t = 0$, there are no concentration gradients throughout the electrolyte. Input parameters for the computational model are taken from Table 1, presented in [19]. Initial salt concentration is set to be 0.16 M, which is close to that found in plasma and interstitial fluids [25]. Initial pH is set to be 7 (neutral). During the OFF-time step the system is solved using as initial conditions the solution obtained from the ON-time step.

The electroporated zone is computed solving the nonlinear Laplace equation with variable conductivity in a sequential way following [26,27]. In silico modeling is validated with measurements as discussed below.

3. Results and discussion

3.1. In vivo modeling

3.1.1. TAM

Fig. 2(a) presents measurements of the normalized electroporated area (NEPA) in TAM (without hyaluronidase: hollow squares, with hyaluronidase: solid squares) vs. electric field E (V/cm). Here, the area (A_E) is normalized by $NEPA = (A_E - A_{0E})/(A_T - A_{0E})$ where A_E is the electroporated area, A_{0E} is the initial electroporated area and A_T is the total area. The figure shows that, as expected, the electroporated area increases with electric field. Fig. 2(b) presents measurements of the

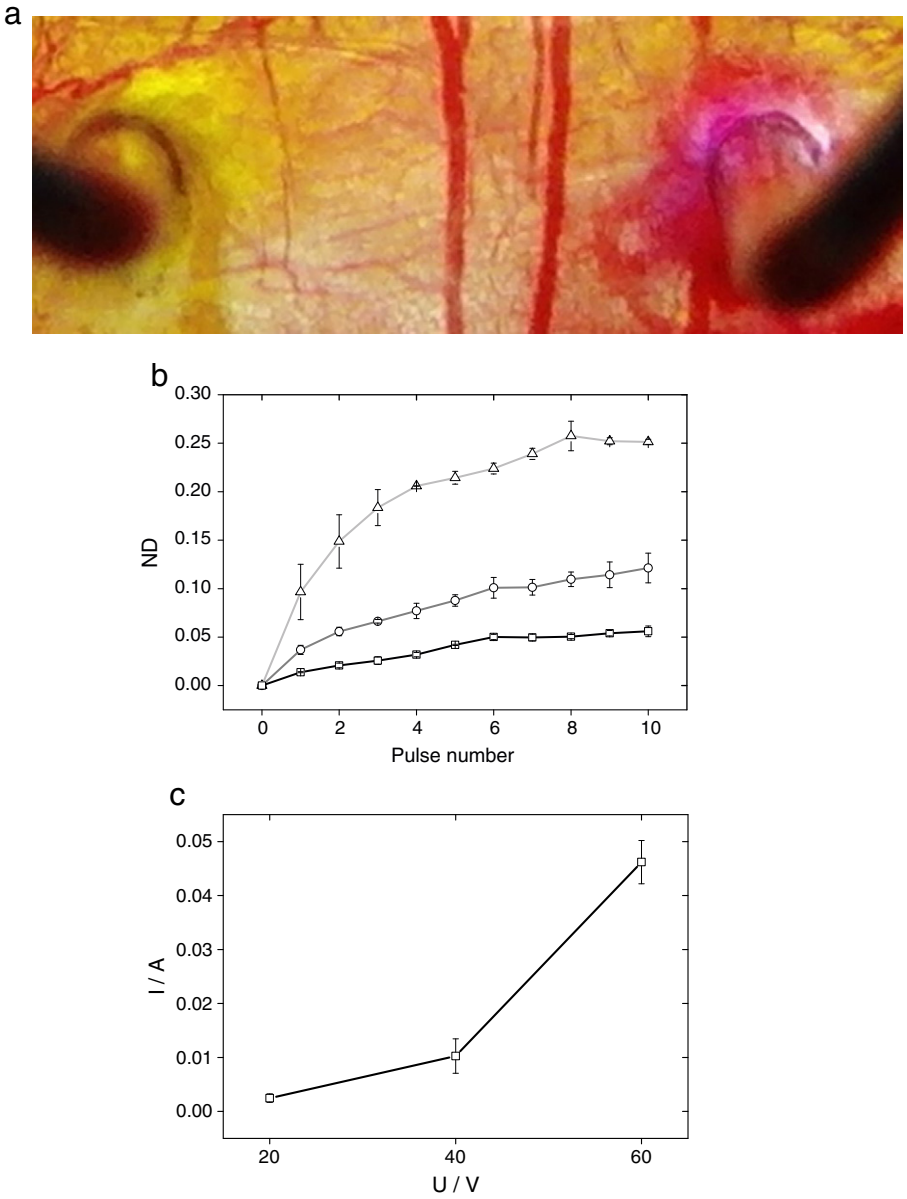

Fig. 3. (a) Anodic and cathodic pH fronts induced by GET in mice observed by intravital microscopy through a DSC: anodic acid front (left electrode) marked with Phenol (red, light yellow area), and cathodic basic front (right electrode) marked with phenolphthalein (pink–red area), during a GET at 200 V/cm. (b) Anodic acid pH fronts in DSC (normalized distance (ND)) vs. pulse number, for different electric fields E (100 (hollow squares), 200 (circles) and 300 (triangles) (V/cm)). (c) Measurements in DSC of the electric current, I (A) vs. voltage U (V).

normalized damaged area (NDA) in TAM (without hyaluronidase) vs. electric field E (V/cm). Here, the area (A_D) is normalized by $NDA = (A_D - A_{0D})/(A_T - A_{0D})$ where A_D is the damaged area and A_{0D} is the initial damaged area. The figure shows that the damaged area, as expected, increases with electric field.

Fig. 2(c) presents electric current in TAM (without hyaluronidase: hollow squares, with hyaluronidase: solid squares) vs. voltage (U/V). The graph shows that electric current increases with voltage and this effect is larger with hyaluronidase; the increase in conductivity due to cell electroporation results in a nonlinear behavior of the current vs. voltage. For the same voltage, the electric current is larger with hyaluronidase than without it, this is caused by a reduction of the electric resistance of the extracellular matrix.

3.1.2. DSC

Fig. 3(a) presents an image of DSC intravital microscopy, showing anodic and cathodic pH fronts induced by GET. The anodic acid front (left electrode) is marked with Phenol (red, light yellow area), and the cathodic basic front (right electrode) with phenolphthalein (pink–red area), during a GET at 200 V/cm. This striking picture is an undeniable evidence of strong pH fronts.

Fig. 3(b) presents a graph of tracked anodic acid pH fronts in a DSC vs. pulse number, for different electric fields E (100 (hollow squares), 200 (circles) and 300 (triangles) V/cm). FITC-Dextran was used as a pH indicator. Here, the distance (D) is normalized by $f(D) = (D - D_0)/(D_T - D_0)$ where D is the sum of the distances covered by pH fronts from their respective electrodes, D_0 is the sum of the initial distance covered by pH fronts from their respective electrodes and D_T is the distance between electrodes. The figure shows that pH front speeds increase with electric field. This is somehow expected since it is well known that pH fronts are proportional to the ion mobility times the electric field.

Fig. 3(c) presents a graph of the electric current I (A) vs. voltage U (V) recorded in a DSC. This graph shows similar trends as those in Fig. 2(c), electric current increases nonlinearly with voltage, due to the increase in the conductivity produced by the electroporation process.

In summary, we have experimentally unveiled the presence of pH fronts emerging from both electrodes and that these fronts can be defined as immediate and substantial due to the qualitative and quantitative evidence presented in Fig. 3(a) and (b). Thermal effects can be discarded according to the experimental work presented in [28–30]. These authors performed a series of in vitro studies with rat biceps femoris muscle. They applied several 0.1 to 10 ms electricfield pulses between 30 V/cm and 150 V/cm to rat muscle held at 10 °C. They found that the maximum temperature rise for the largest combination of pulse width and electric field amplitude was 8 °C, a clearly nonpathologic temperature peak (≤20 °C). It has been suggested that IRE damage could be observed due to strong electric fields in a zone very near the electrodes. We used a GET protocol which in theory cannot produce IRE damage, however, if a tissue inhomogeneity exists in a very small region near the electrodes, GET conditions might not be satisfied and minimal IRE damage could arise. If this damage exists, it is negligible compared to the total damage produced in the tissue by pH and could be disregarded. This is because in a GET protocol the electric field applied is always below the electric field producing IRE damage (more about this in Section 3.2.2).

Accordingly, since thermal effects can be discarded, pH fronts presented in Fig. 3(a) and quantified in Fig. 3(b) appear to be the main cause of muscle damage observed in TAM using hyaluronidase + GET protocols.

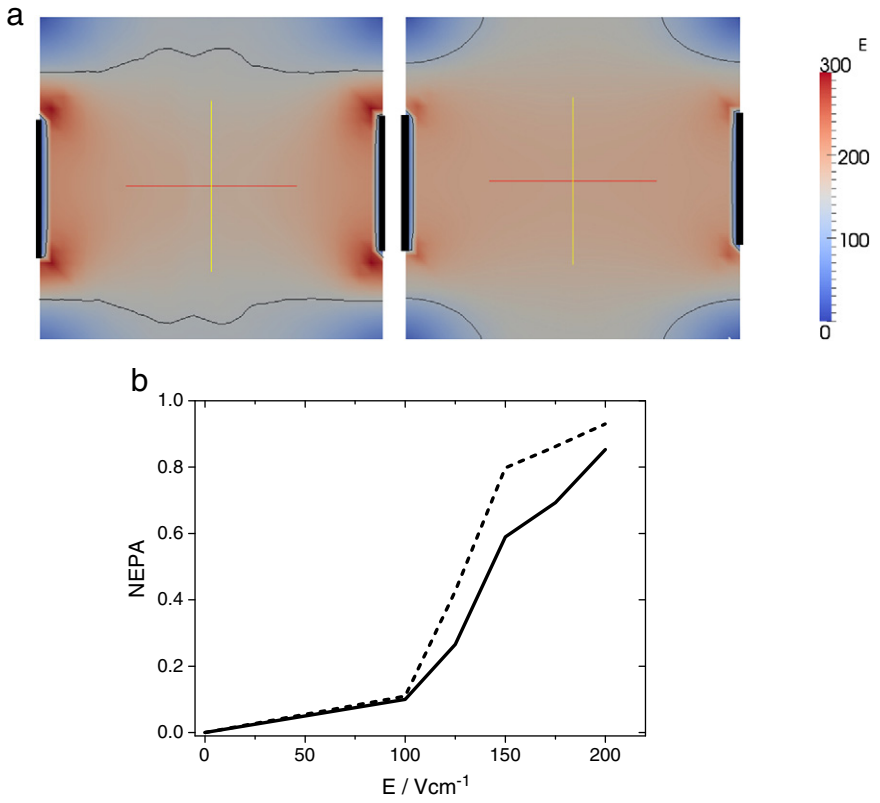

Fig. 4. Predicted electroporated area (black contouring lines) and electric field variation (red brown contouring) at a cross section through electrode centers for an applied electric field of 175 V/cm (figure (a)). Figure (a) (left) is without hyaluronidase, figure (a) (right) with hyaluronidase. (b) Normalized electroporated area (NEPA) (with hyaluronidase depicted with a dotted line and without depicted with a solid line) vs. electric field E (V/cm).

3.2. In silico modeling

3.2.1. TAM

Fig. 4a presents predicted electroporated area (black contouring lines) and electric field variation (red brown contouring) at a cross section through electrode centers for an applied electric field of 175 V/cm. Fig. 4(a) (left) is without hyaluronidase and Fig. 4(a) (right) is with hyaluronidase. Comparing left and right images shows that without hyaluronidase the electric field variation is much larger near the electrodes, the effect of hyaluronidase being a smoothing of the electric field as seen in the right image. Contrarily, with hyaluronidase the electroporated area is larger.

Fig. 4(b) presents predicted NEPA (with and without hyaluronidase) vs. electric field E (V/cm). Without hyaluronidase trends are similar to measurements presented in Fig. 2(a). As expected, electroporated area is larger with hyaluronidase.

3.2.2. DSC

Fig. 5(a) and (b) presents predicted anodic acid pH fronts vs. distance to the anode D (mm) for different electric fields E (50 (solid line), 150 (dashed line), 175 (dashed-dashed line) and 200 (dotted line) V/cm), without and with hyaluronidase, respectively (we note that results with hyaluronidase are presented here for a comparison purpose, however, they are intended to simulate a TAM experiment). By computing the pH distribution in a given region the damaged area

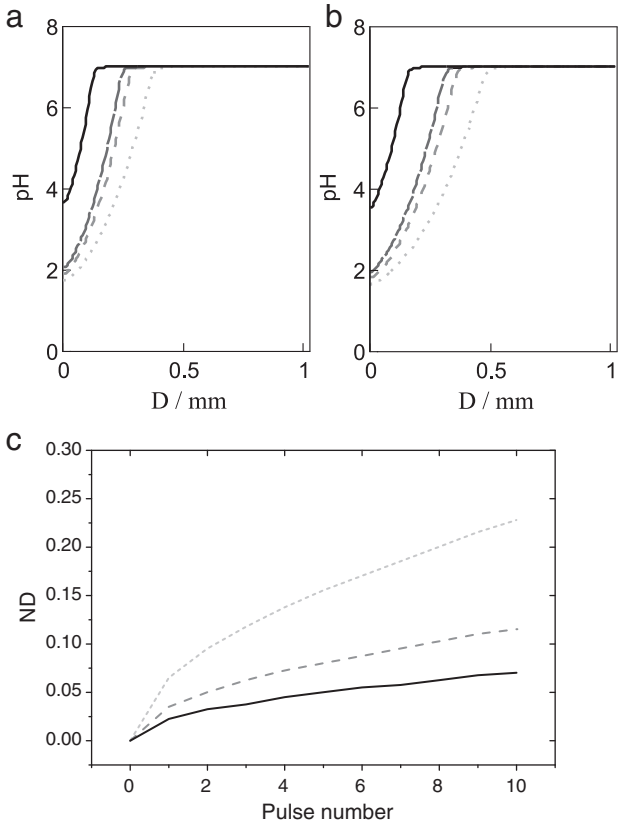

Fig. 5. (a) and (b) Anodic acid pH fronts vs. distance D (mm) (distance to the anode) for various electric fields E (50 (solid line), 150 (dashed line), 175 (dashed-dashed line) and 200 (dotted line) V/cm), without and with hyaluronidase, respectively (we note that results with hyaluronidase are presented here for a comparison purpose, however, they are intended to simulate a TAM experiment. (c) Anodic acid pH front normalized distance (ND) vs. pulse numbers, for different electric fields (100 (solid line), 200 (dash line) and 300 (dot line) V/cm).

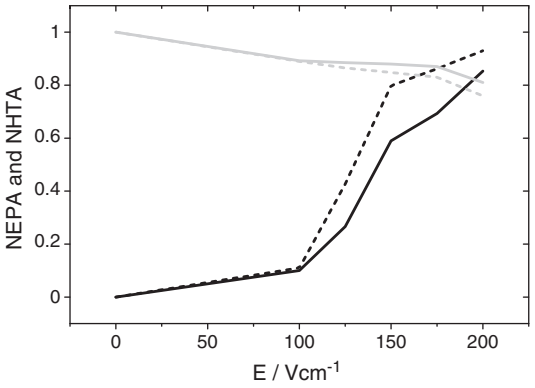

Fig. 6. Normalized healthy tissue area (NHTA) with hyaluronidase (dashed gray line) and without (solid gray line) vs. electric field E (V/cm), and predicted NEPA with hyaluronidase (dashed black line) and without (solid black line) vs. electric field E (V/cm).

in that region is obtained, thus the healthy region area (here we assume that the healthy area is the complement of the damaged area). The damaged area is defined as the area in which pH values are above 8.5 or below, 5.5. The healthy area falls within the interval 5.5 and 8.5. Fig. 5(a) and (b) shows that larger electric fields determine larger acidic areas. Moreover, with hyaluronidase, the damaged area is slightly extended, this is because electric current is increased, thus pH effects. Fig. 5(c) presents predicted anodic acid pH front normalized distance (ND) vs. pulse numbers for different electric fields E (100 (solid line), 200 (dashed line) and 300 (dotted line) V/cm). As shown in the figure, predictions come close to measurements (see Fig. 3(b)).

In summary, we have theoretically demonstrated the existence of pH fronts emerging from both electrodes and that these fronts are immediate and substantial as observed in Fig. 5. Thermal effects can also be discarded because GET pulses are below IRE pulses which, as demonstrated by [31] have no thermal effects. As previously mentioned, in an in vivo GET modeling, IRE damage near the electrodes was disregarded as compared to the total pH damage. In an in silico GET modeling, if IRE damage exists due to a tissue inhomogeneity near the electrodes, it is considered minimum. This is because the electric field applied is always below that producing IRE damage. In an in silico hyaluronidase + GET modeling, the electric field is smaller but the damage is greater, this can only be attributed to pH damage. Therefore, if IRE damage exists it can be disregarded as compared to the total pH damage. In summary, theoretical predictions show that in a GET protocol, whether with or without hyaluronidase, electric fields produced are below those inducing IRE, therefore pH fronts are the principal cause of tissue damage. From this we can infer that pH fronts are the main cause of muscle damage observed in the TAM hyaluronidase + GET experiments.

Finally, with the goal of determining an optimal GET protocol, Fig. 6 presents normalized healthy tissue (NHTA) with hyaluronidase (dashed gray line) and without (continuous gray line) vs. electric field E (V/cm), and normalized electroporated area with hyaluronidase (dashed black line) and without (solid black line) vs. electric field E (V/cm). This figure shows two competing sides of the addition of hyaluronidase in the GET protocol. On one side, with hyaluronidase, electroporated area is larger than without. In other terms, with hyaluronidase the same electroporated area is obtained with less intense electric fields. On the other side, with hyaluronidase, electric current is higher, thus pH effects are higher with the associated tissue damage. These competing sides are reflected in Fig. 6 that suggests that optimum GET protocols are obtained with electric field values of 158 V/cm and 183 V/cm with and without hyaluronidase, respectively. Consequently, although in hyaluronidase + GET protocols transgene uptake and expression are greatly maximized, the use of hyaluronidase induces greater damage near the electrodes.

4. Conclusions

In this work we presented in vivo and in silico modeling evidence proving the role of pH in the tissue damage observed during the application of a GET protocol with or without hyaluronidase pretreatment. Experiments unveil the presence of pH fronts and that these fronts are immediate and substantial thus giving rise to tissue necrosis. Theory confirms experiments and shows that in GET protocols whether with or without hyaluronidase pretreatment, pH fronts are the principal cause of muscle damage near the electrodes. It also demonstrates that at constant voltage, the presence of hyaluronidase renders the tissue more conductive, in turn increasing electric current, thus pH effects. Consequently, although in hyaluronidase + GET protocols transgene uptake and expression are greatly maximized, the use of hyaluronidase induces greater damage near the electrodes. A theoretical framework is presented in which it is possible to select electric field parameters optimizing GET protocols by taking into account pH effects.

GET is emerging as a promising approach for its application in human patients. Currently, many clinical trials are under investigation: phase I and some phase II protocols, based on DNA vaccination mediated by electrotransfer, are being applied against not only in infectious diseases but also in cancer. They are designed to test safety and efficacy of GET in order to make this strategy useful and applicable in the future [32]. For this reason, the study of the mechanisms and strategies to improve these protocols is a crucial step in the biomedical-engineering research field.

Acknowledgments

E. Signori is grateful and thanks Prof DJ Wells. F. Maglietti and S. Michinski have scholarships from Consejo Nacional de Investigaciones Científicas y Técnicas (CONICET) and Instituto Tecnológico Buenos Aires (ITBA), respectively. P. Turjanski, N. Olaiz, C. Suárez, A. Soba and G. Marshall are members from CONICET. This work was supported by grants from Universidad de Buenos Aires (UBACyT X132/08), CONICET (PIP 112-200801-01087/09), MINCyT (SLO-AR 08/02/09), ITBACyT 2012 (modalidad I, Nro 1) and Biomedicine and Molecular Biosciences COST Action TD1104.

References

[1] D. Miklavčič, Network for development of electroporation-based technologies and treatments: COST TD1104, J. Membr. Biol. 245 (2012) 591–598.
[2] S. Orlowski, L. Mir, Cell electropermeabilization: a new tool for biochemical and pharmacological studies, Biochim. Biophys. Acta Rev. Biomembr. 1154 (1993) 51–63.
[3] L. Mir, Bases and rationale of the electrochemotherapy, Eur. J. Cancer Suppl. 4 (2006) 38–44.
[4] J.C. Weaver, Electroporation: a general phenomenon for manipulating cells and tissues, J. Cell. Biochem. 51 (1993) 426–435 (PMID: 8496245).
[5] R. Davalos, L. Mir, B. Rubinsky, Tissue ablation with irreversible electroporation, Ann. Biomed. Eng. 33 (2005) 223–231.
[6] E. Neumann, M. Schaefer-Ridder, Y. Wang, P. Hofschneider, Gene transfer into mouse glioma cells by electroporation in high electric fields, EMBO J. 1 (1982) 841–845.
[7] T.K. Wong, E. Neumann, Electric field mediated gene transfer, Biochem. Biophys. Res. Commun. 107 (1982) 584–587 (PMID: 7126230).
[8] J.-M. Escoffre, T. Portet, L. Wasungu, J. Teissié, D. Dean, M.-P. Rols, What is (still not) known of the mechanism by which electroporation mediates gene transfer and expression in cells and tissues, Mol. Biotechnol. 41 (2008) 286–295.
[9] M. Pavlin, K. Flisar, M. KanduÅ¡er, The role of electrophoresis in gene electrotransfer, J. Membr. Biol. 236 (2010) 75–79.
[10] H. Shirota, L. Petrenko, C. Hong, D.M. Klinman, Potential of transfected muscle cells to contribute to DNA vaccine immunogenicity, J. Immunol. 179 (2007) 329–336.
[11] P. Chiarella, E. Massi, M. De Robertis, A. Sibilio, P. Parrella, V.M. Fazio, E. Signori, Electroporation of skeletal muscle induces danger signal release and antigen-presenting cell recruitment independently of DNA vaccine administration, Expert. Opin. Biol. Ther. 8 (2008) 1645–1657 (PMID: 18847301).
[12] P. Chiarella, V.M. Fazio, E. Signori, Application of electroporation in DNA vaccination protocols, Curr. Gene Ther. 10 (2010) 281–286 (PMID: 20504275).
[13] J.M. McMahon, E. Signori, K.E. Wells, V.M. Fazio, D.J. Wells, Optimisation of electrotransfer of plasmid into skeletal muscle by pretreatment with hyaluronidase — increased expression with reduced muscle damage, Gene Ther. 8 (2001) 1264–1270 (PMID: 11509960).
[14] P. Chiarella, S. De Santis, V.M. Fazio, E. Signori, Hyaluronidase contributes to early inflammatory events induced by electrotransfer in mouse skeletal muscle, Hum. Gene Ther. 24 (2013) 406–416 (PMID: 23360544).
[15] R. Stern, M.J. Jedrzejas, Hyaluronidases: their genomics, structures, and mechanisms of action, Chem. Rev. 106 (2006) 818–839.
[16] N. Olaiz, F. Maglietti, C. Suárez, F. Molina, D. Miklavcicc, L. Mir, G. Marshall, Electrochemical treatment of tumors using a one-probe two-electrode device, Electrochim. Acta 55 (2010) 6010–6014.
[17] N. Olaiz, C. Suárez, M. Risk, F. Molina, G. Marshall, Tracking protein electrodenaturation fronts in the electrochemical treatment of tumors, Electrochem. Commun. 12 (2010) 1388–2481.
[18] P. Turjanski, N. Olaiz, P. Abou-Adal, C. Suárez, M. Risk, G. Marshall, ph front tracking in the electrochemical treatment (EChT) of tumors: experiments and simulations, Electrochim. Acta 54 (2009) 6199–6206.
[19] P. Turjanski, N. Olaiz, F. Maglietti, S. Michinski, G. Marshall, The role of ph fronts in reversible electroporation, PLoS ONE 6 (2011) e17303.
[20] F. Maglietti, S. Michinski, N. Olaiz, M. Castro, C. Suárez, G. Marshall, The role of ph fronts in tissue electroporation based treatments, PLoS ONE 8 (2013) e80167.
[21] J.D. Vry, P. Martínez-Martínez, M. Losen, G.H. Bode, Y. Temel, T. Steckler, H.W. Steinbusch, M.D. Baets, J. Prickaerts, Low current-driven micro-electroporation allows efficient in vivo delivery of nonviral DNA into the adult mouse brain, Mol. Ther. J. Am. Soc. Gene Ther. (2010), http://www.ncbi.nlm.nih.gov/pubmed/?term=Low+current-+driven+micro-electroporation+allows+e%0Ecient+in+vivo+delivery+of+nonviral+DNA+into+the+adult+mouse+brain%2C (PMID: 20389292).
[22] E. Bellard, B. Markelc, S. Pelofy, F. Le Guerroué, G. Sersa, J. Teissié, M. Cemazar, M. Golzio, Intravital microscopy at the single vessel level brings new insights of vascular modification mechanisms induced by electropermeabilization, Off. J. Controlled Release Soc. 163 (2012) 396–403 (PMID: 23017380).
[23] B. Markelc, G. Sersa, M. Cemazar, Differential mechanisms associated with vascular disrupting action of electrochemotherapy: intravital microscopy on the level of single normal and tumor blood vessels, PLoS ONE 8 (2013) e59557.
[24] G. Marshall, Solución Numérica de Ecuaciones Diferenciales, Tomo II: Ecuaciones en Derivadas Parciales, Editorial Reverté S.A., Buenos Aires, 1986.
[25] J. West, Physiological Basis of Medical Practice, 11th ed. Lippincott, William & Wilkins, Baltimore, 1985.
[26] D. Sel, D. Cukjati, D. Batiuskaite, T. Slivnik, L.M. Mir, D. Miklavčič, Sequential finite element model of tissue electropermeabilization, IEEE Trans. Biomed. Eng. 52 (2005) 816–827.
[27] S. Corović, M. Pavlin, D. Miklavčič, Analytical and numerical quantification and comparison of the local electric field in the tissue for different electrode configurations, Biomed. Eng. Online 15 (2007) 6–37.
[28] R.C. Lee, D. Zhang, J. Hannig, Biophysical injury mechanisms in electrical shock trauma, Annu. Rev. Biomed. Eng. 2 (2000) 477–509.
[29] R.C. Lee, Injury by electrical forces: pathophysiology, manifestations, and therapy, Curr. Probl. Surg. 34 (1997) 677–764.
[30] D.L. Bhatt, D.C. Gaylor, R.C. Lee, Rhabdomyolysis due to pulsed electric fields, Plast. Reconstr. Surg. 86 (1990) 1–11 (PMID: 2359775).
[31] P.A. Garcia, J.H. Rossmeisl, R.E. Neal, T.L. Ellis, R.V. Davalos, A parametric study delineating irreversible electroporation from thermal damage based on a minimally invasive intracranial procedure, BioMed. Eng. OnLine 10 (2011) 34.
[32] P. Chiarella, V.M. Fazio, E. Signori, Electroporation in DNA vaccination protocols against cancer, Curr. Drug Metab. 14 (2013) 291–299 (PMID: 23116110).